ELSEVIER

NeuroImage

www.elsevier.com/locate/ynimg
NeuroImage 30 (2006) 857 – 870

Transcranial magnetic stimulation and stroke: A computer-based human model study

Tim Wagner,[a,b,c,*] Felipe Fregni,[a] Uri Eden,[c] Ciro Ramos-Estebanez,[a] Alan Grodzinsky,[b,d] Markus Zahn,[b] and Alvaro Pascual-Leone[a]

[a]*Center for Non-Invasive Brain Stimulation, Beth Israel Deaconess Medical Center, Harvard Medical School, Boston, MA 02215, USA*
[b]*Department of Electrical Engineering and Computer Science, Massachusetts Institute of Technology, Cambridge, MA 02132, USA*
[c]*Division of Health Sciences and Technology, Harvard Medical School/Massachusetts Institute of Technology, Boston, MA 02108, USA*
[d]*Center for Biomedical Engineering, Massachusetts Institute of Technology, Cambridge, MA 02108, USA*

Received 2 February 2005; revised 11 April 2005; accepted 15 April 2005
Available online 13 February 2006

This paper explores how transcranial magnetic stimulation (TMS) induced currents in the brain are perturbed by electrical and anatomical changes following a stroke in its chronic stage. Multiple MRI derived finite element head models were constructed and evaluated to address the effects that strokes can have on the induced stimulating TMS currents by comparing stroke models of various sizes and geometries to a healthy head model under a number of stimulation conditions. The TMS induced currents were significantly altered for stimulation proximal to the lesion site in all of the models analyzed. The current density distributions were modified in magnitude, location, and orientation such that the population of neural elements that are stimulated will be correspondingly altered. The current perturbations were minimized for conditions tested where the coil was far removed from the lesion site, including models of stimulation contralateral to the lesioned hemisphere. The present limitations of TMS to the peri-lesional cortex are explored, ultimately concluding that conventional clinical standards for stimulation are unreliable and potentially dangerous predictors of the site and degree of stimulation when TMS is applied proximal to infarction site.

Keywords: Stroke rehabilitation; Finite element model; Transcranial magnetic stimulation

Introduction

Transcranial magnetic stimulation (TMS) is a powerful tool used to study brain function non-invasively. With TMS, a current carrying coil generates a pulsed magnetic field that can induce stimulating currents in the underlying neural tissue. Repetitive TMS (rTMS) can alter cortical function beyond the train of stimulation (Pascual-Leone et al., 1999). For example, rTMS of the motor cortex can modify the motor-evoked potentials (MEPs) for minutes or even hours after the rTMS (Bohning et al., 1997; Romero et al., 2002). Applied to other cortical regions, rTMS can lead to observable behavioral effects, presumably by modulating excitability in the targeted cortical region and its connected neural network (Gangitano et al., 2002; Hilgetag et al., 2001; Kosslyn et al., 1999; Theoret et al., 2001).

Since its inception, TMS has been widely used as a tool in stroke research for diagnostic, prognostic, and even therapeutic applications. TMS was first used in stroke patients in 1990 (Eisen and Shtybel, 1990). Since that time, several studies have been published using TMS as a diagnostic tool (Berardelli, 1991; Dachy and Dan, 2002; Schwarz et al., 2000; Urban et al., 2002; Werhahn et al., 1995), prognostic tool (Arac et al., 1994; Cruz Martinez et al., 1999; D'Olhaberriague et al., 1997; Dachy et al., 2003; Escudero et al., 1998; Ferbert and Buchner, 1991; Hendricks et al., 2002; Muellbacher and Mamoli, 1995; Nardone and Tezzon, 2002; Pennisi et al., 1999; Pereon et al., 1995; Rapisarda et al., 1996; Rossini, 2000; Stulin et al., 2003; Traversa et al., 1998; Vang et al., 1999), and investigative tool for stroke pathophysiology (Byrnes et al., 1999; Cicinelli et al., 1997; Delvaux et al., 2003; Gomez-Fernandez, 2000; Wittenberg et al., 2003). In addition, the modulatory characteristics of rTMS render it a realistic and promising technique to treat brain dysfunction after stroke (Mansur et al., 2005; Martin et al., 2004).

However, to date, there has been no systematic study of the effects that strokes can have on perturbing the currents induced by TMS in the neural tissue, despite the well-known fact that after a stroke, numerous physiologic changes occur in the brain tissue, which can alter its electrical response properties. Necrotic brain tissue in the infarction region is phagocytized by inflammatory cells and replaced by a cerebral spinal fluid (CSF) filled network of astrocytes and glial fibers (De Girolami et al., 1999). The degree to which the infarction region fills with CSF is dependent on the

* Corresponding author. Center for Non-Invasive Brain Stimulation, 330 Brookline Ave. # KS452, Boston, MA 02215, USA. Fax: +1 617 975 5322.
E-mail address: twagner@mit.edu (T. Wagner).
Available online on ScienceDirect (www.sciencedirect.com).

1053-8119/$ - see front matter © 2005 Elsevier Inc. All rights reserved.
doi:10.1016/j.neuroimage.2005.04.046

degree of damage (Jacobs et al., 2001; Soltanian-Zadeh et al., 2003). This CSF influx represents a six-fold increase in conductance in the infarction region and a drastic modification to the tissue geometry and conductive matrix of the region (Wagner et al., 2004). In TMS, similar changes in tissue geometry and electromagnetic properties have been shown to alter the induced stimulating currents in both phantom and modeling studies (Yunokuchi et al., 1998; Liu and Ueno, 2000; Wagner et al., 2004). Herein, we explore the question of how the induced currents in the brain are perturbed by electrical and anatomical changes following a stroke in its chronic stage (i.e., 30 days post-cerebral–vascular incident (Sironi et al., 2004)). We also discuss the possible clinical implications of the perturbations to the current induced under TMS in patients with stroke.

Methods

Models

Multiple MRI derived finite element head models were constructed and evaluated for various stimulation orientations to address the effects that strokes can have on perturbing the induced stimulating TMS current.

MRI guided finite element head model

An initial sinusoidal steady-state finite element model (FEM) was developed using the Ansoft 3 D Field Simulator software package with the eddy current solver (Ansoft, 2002). We used an MRI guided three-dimensional CAD rendering of the human head to solve for the currents induced in the cortex during magnetic stimulation (Wagner et al., 2004). We refer to this as the healthy head model (see Fig. 1). This model was generated to include the skin, skull, CSF, and cerebral tissue. The tissue conductivities, while somewhat attenuated below 1-kHz stimulation frequencies (Dissado, 1990), were considered essentially constant for the frequencies of TMS (the power spectrum of typical stimulators is composed of components less than 10 kHz (Cerri et al, 1995)). The greatest variability existed in the referenced values for the skin conductivity, most likely due to unaccounted anisotropies; however, all the tissues were considered isotropic and homogenous for this model. Thus, the tissue conductivities in the model were assigned the mean value from multiple references; skin at 0.465 S/m, bone at 0.010 S/m, CSF at 1.654 S/m, and cerebral tissue at 0.276 S/m (see Table 1 and Appendix, Table 1-S, references included in table).

The actual low-frequency permittivity value of biological tissues is an area of ongoing investigation, where a trend of increasing tissue permittivity with decreased frequency has been reported in the literature (Dissado, 1990; Foster and Schwan, 1996; Hart et al., 1996; Pethig and Kell, 1987). Nevertheless, there is limited consensus on the exact value of the relative permittivity magnitudes in biological tissues. However, magnitudes in excess of the order 10^4 ε_o are infrequently encountered in the range of peak TMS source frequencies. Thus, in this present study, the tissue permittivities were such that the displacement currents had a negligible effect in the calculation of the induced current density distributions (Wagner et al., 2004). Even though the tissue permittivities had a negligible effect on this study, they were included in this model and assigned values reflective of trends in the literature (see Table 1).

The source was modeled as a figure of eight coil with two 3.5-cm radius windings made of a single turn of 7-mm radius copper wire. The copper was modeled as a perfect conductor (currents constrained to the surface) with the permittivity set to ε_o, conductivity of 5.8×10^7 S/m and a permeability of 1.0 μ_o. The source current was set at 5 kHz with a 1.8×10^3 A peak current (5.65×10^7 A/s, rate of change of the peak current with time). The 5-kHz frequency component of the source was chosen based on the peak frequency component seen in the power spectrum of the commercially available Magstim Rapid Stimulator (Magstim). Unless otherwise noted, for each solution obtained, the coil was positioned with its facial plane tangential to the scalp, with its plane of symmetry (containing the coil handle) at an approximate 30° angle to the normal from the most lateral edge of the scalp surface, and with its facial plane 7 mm above the scalp surface to account for the insulating layer found in commercially available coils (Jalinous, 1991).

The FEM solver implemented a modified T-Ω method (Ansoft, 1990a,b; Starzynski et al., 2002; Wagner et al., 2004) to solve for the induced current densities. The Ansoft FEM solver was set to follow an adaptive iterative process with convergence limits determined by the energy error in the system, further detailed in an earlier article (Wagner et al., 2004). The criterion for model convergence was defined as an energy error below 1.0%.

The magnitude and location of the maximum cortical current density were evaluated for each coil position tested for the healthy head model. Additionally, the surface area on the cortex where the current density was greater than 90% of its maximum value was calculated (i.e., if the maximum magnitude of the cortical current density was 1 A/m^2 for coil position X, then the area was calculated where the current ranged from 0.9 to 1.0 A/m^2); we will refer to this as the maximum cortical current surface area. Furthermore, the induced current density vector behavior was also analyzed in the tissues. Where the results are reported as current density magnitudes, they indicate the magnitude of the sinusoidal steady-state current density $\vec{J}(x,y,z)$ in the units of A/m^2, unless otherwise noted. Additionally the x, y, z coordinate system used in this paper is defined in Fig. 1F and uses mm units.

Stroke models

We implemented 11 different stroke models of various sizes and geometries to compare to the healthy head model under different conditions. These stroke models were constructed by altering the healthy head model's cortical geometry guided by the brain MRIs of patients with cortical strokes treated at Beth Israel Deaconess Medical Center. Strokes were chosen based on the different infarction volume and dimensions. To represent the infarction site in the FEM construction, CSF was used to replace the damaged tissue as shown by imaging and histopathology studies in the post acute stage (Jacobs et al., 2001; Soltanian-Zadeh et al., 2003). The edges of the stroke were smoothed in the stroke model construction, and the stroke volumes were considered homogeneous, excluding islands of cortical tissue inside the stroke regions. Stroke 1 had an approximate volume of 18.5 cm^3 and was located in the right frontal lobe due to an infarction of superior branches of the right middle cerebral artery with a maximum 2.5 cm inferior to superior length along the cortical face, a maximum 3.5 cm anterior to posterior length along the cortical face, and a maximum depth of 2.8 cm measured from the cortical face (see Figs. 1A and B). Strokes 2A–2C were all located in the right frontal lobe due to

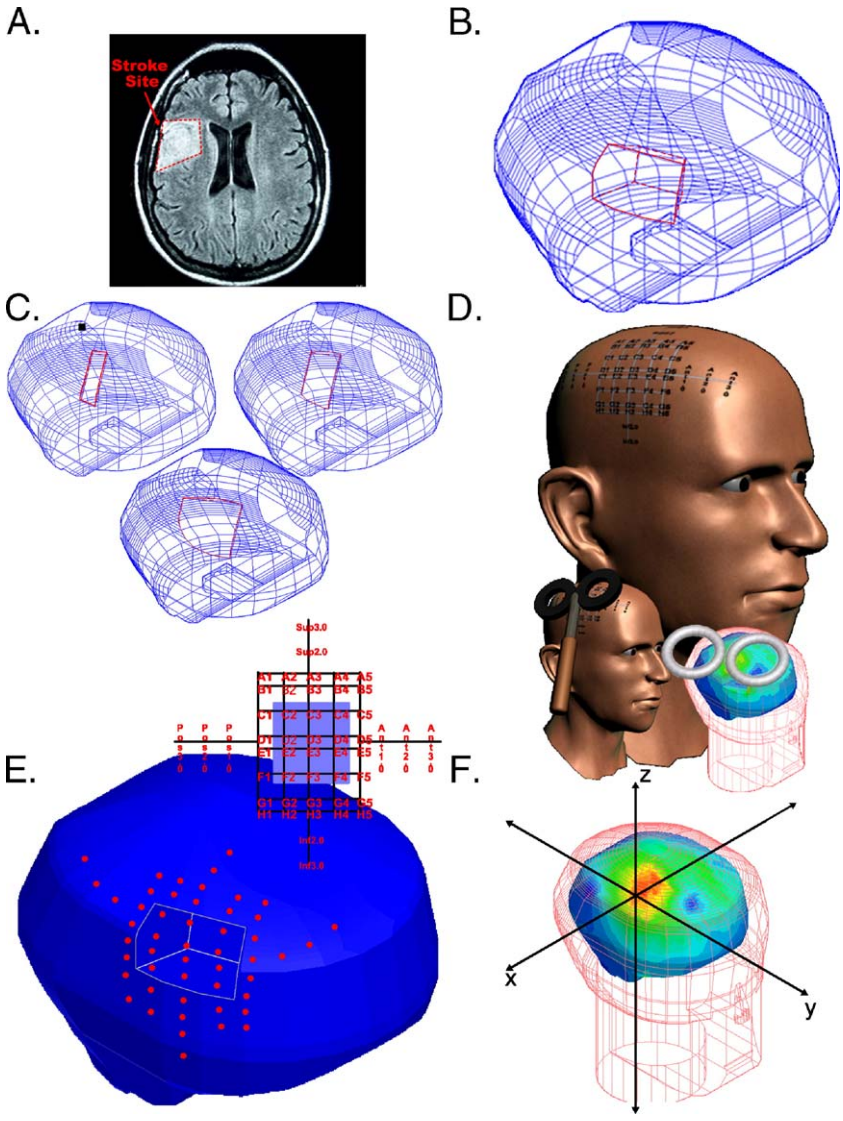

Fig. 1. Geometries: (A) Stroke 1 MRI transverse slice. (B) Stroke 1 model cortical mesh highlighting the location of the infarction site. In Stroke 1 model, the infarction site is replaced by CSF. In the healthy head model, the infarction site is not present. (C) Strokes 2A–C models cortical mesh highlighting the locations of the corresponding infarction sites. (D) Surface grid on scalp surface while the inset shows both the coil in the A1 position and the corresponding FEM skin surface with an underlying plotted cortical surface current density. (E) Grid projection on the cortical surface with a flat projection of the surface grid in the foreground, note the light blue box highlights the infarction face outline. (F) Model coordinate system, here shown with the healthy head model—the same coordinate system was used for all the models, note that the current density magnitude solution is for a reference shown where the solution is that of the healthy head model in the B1 coil position.

infarctions of superior branches of the right middle cerebral artery with approximate volumes of 1.3 cm^3, 2.6 cm^3, and 5.3 cm^3 respectively. Strokes 2A–2C all shared maximum depths of 4 mm measured from the cortical face, 4 cm inferior to superior lengths along the cortical face, and a 1 cm, 2 cm, and 4 cm anterior to posterior length along the cortical face respectively (see Fig. 1C). Strokes 3A–3C were all located in the right frontal lobe due to infarctions of superior branches of the right middle cerebral artery with approximate volumes of 2.6 cm^3, 5.3 cm^3, and 10.6 cm^3 respectively. Strokes 3A–3C all shared maximum depths of 8 mm measured from the cortical face, 4 cm inferior to superior lengths along the cortical face, and a 1 cm, 2 cm, and 4 cm anterior to posterior length along the cortical face respectively. Strokes 2A–2C differed primarily by depth from the corresponding Strokes 3A–3C models (i.e., Stroke 2A and Stroke 3A shared the same shape along the cortical face but differed by the maximum depth, see Fig. 1C). Strokes 4A–4C were all located in the right frontal lobe due to infarctions of superior branches of the right middle cerebral artery

Table 1
Mean conductivity values and relative permittivity schemes used

Tissue	Mean conductivity (S/m)	Relative permittivity scheme (F/m)
Skin–scalp	0.465	1.2×10^4 ε_o
Bone–skull	0.010	0.8×10^4 ε_o
Cerebral spinal fluid	1.654	0.60×10^4 ε_o
Cerebral tissue	0.276	1.2×10^4 ε_o

with approximate volumes of 5.3 cm^3, 10.6 cm^3, and 21.2 cm^3 respectively. Strokes 4A–4C all shared maximum depths of 12 mm measured from the cortical face, 4 cm inferior to superior lengths along the cortical face, and a 1 cm, 2 cm, and 4 cm anterior to posterior length along the cortical face respectively. Strokes 4A–4C differed primarily by depth from the corresponding Strokes 2A–2C and 3A–3C models. Additionally, the infarction sites for Stroke models 2–4 (Strokes 2A–2C, Strokes 3A–3C, Strokes 4A–4C) were normalized in location to share the same center on the model's cortical face. Finally, Stroke 5 represented a large stroke due to left MCA occlusion; its size was approximately 350 cm^3 and was designed by removing the left cortical hemisphere from the model. The stroke models differed from the healthy head model only at the infarction location, where the electrical properties corresponded to that of CSF at the infarction site as opposed to gray matter, and were identical to the healthy head model outside the stroke region (both geometrically and electrically). The stroke dimensions are tabulated in Table 2.

We analyzed the magnitude of the maximum cortical current density, the location of the maximum cortical current density, the maximum cortical current surface area, and the induced current density vector behavior for each of the coil positions in the stroke models.

The stroke solutions were then compared to the analogous healthy head models. The number of cortical areas in the stroke models where current density magnitudes were found to be in excess of 100%, 120%, and 150% of the maximum cortical current density in the corresponding healthy head model was calculated. For each of these areas, the location, the maximum current density magnitude in the area, and the cortical surface area were also calculated.

Analyses

Specific tests were conducted to explore the effects of the relative coil to stroke location, the infarction size and shape, and large contralateral strokes can have on the induced stimulating currents.

Effects of relative coil location on the induced stimulating currents

In order to investigate the effects of the coil location on the induced stimulating current, solutions were obtained for both the healthy head model and Stroke 1 model with the coil center placed at locations along a grid on the scalp surface (see Fig. 1D). As the exact location of the maximum current density on the cortex could not be predicted prior to solving the problem, the coil locations were chosen based on the site of the normal projection from the figure of eight coil's center on the scalp surface to the cortical surface (much like the prediction method used in many commercially available frameless stereotactic systems), with enough locations to broadly encompass the stroke border and allow for the testing of locations both inside (12 locations) and outside (38 locations) the infarction region. Points A1–A5 are located along a horizontal line that transverses the scalp surface such that their projections are approximately 1 cm superior to the superior stroke border. Similarly, the projection of points B1–B5 and C1–C5 is approximately 0.5 cm superior and 0.5 cm inferior to the superior stroke border respectively. The projection of D1–D5 and E1–E5 is 0.5 cm superior and 0.5 cm inferior to the horizontal midline of the stroke outline. Finally, the projection of points F1–F5, G1–G5, and H1–H5 is 0.5 cm superior, 0.5 cm inferior, and 1 cm inferior to the inferior stroke border. A similar arrangement exists for the projections of each of the vertical lines in the grid (A1–H1 through A5–H5) with reference to the anterior stroke border, vertical midline, and posterior stroke border. Additional locations were evaluated outside the grid border: three locations approximately 1.0 cm, 2.0 cm, and 3.0 cm posterior to the horizontal center of the posterior stroke border, and anterior to the horizontal center of the anterior stroke border, and two locations approximately 2.0 cm and 3.0 cm superior to the vertical center of the superior stroke border, and inferior to the vertical center of the inferior stroke border. We shall refer to these locations using the abbreviated position (Ant, Pos, Sup, Inf) and the distance so that Ant1.0 refers to the anterior point 1 cm from the anterior stroke border. One hundred total locations were evaluated, fifty for each of the Stroke 1 and the healthy head models (see Figs. 1D and E for the scalp surface grid and the cortical projections, Appendix, Table 2-S, tabulates all of the coil center positions on the scalp, and Fig. 1F defines the coordinate system used for all of the models).

Table 2
Stroke geometries

Stroke model	Maximum anterior to posterior width (mm)	Maximum inferior to superior length (mm)	Maximum depth (mm)
Stroke 1	35	25	28
Stroke 2A	10	40	4
Stroke 2B	20	40	4
Stroke 2C	40	40	4
Stroke 3A	10	40	8
Stroke 3B	20	40	8
Stroke 3C	40	40	8
Stroke 4A	10	40	12
Stroke 4B	20	40	12
Stroke 4C	40	40	12
Stroke 5	Left hemisphere removed		

Effects of the infarction size on the induced stimulating currents

In order to investigate the effects of the infarction size and shape on the induced stimulating current, solutions to the FEM model were obtained for Strokes 2A, 2B, 2C, 3A, 3B, 3C, 4A, 4B, and 4C and compared to the healthy head model with the normal projection from coil's center located over the center of infarction's cortical face and located approximately 0.5 cm posterior to the posterior border of each infarction. The coil position referred to as CPCenter corresponded to the center of the strokes' cortical faces (figure of eight coil centered at (−9, −3, −14) on the skin surface). CPA was 0.5 cm posterior from the Strokes 2A, 3A, and 4A's infarction border (figure of eight coil centered at (−9, −15, −12) on the skin surface). CPB was 0.5 cm posterior from Strokes 2B, 3B, and 4B's infarction border (figure of eight coil centered at (−6, −20, −13) on the skin surface). And CPC was 0.5 cm posterior from the Strokes 2C, 3C, and 4C's infarction border (figure of eight coil centered at (−5, −25, −14) on the skin surface).

Effects of contralateral hemisphere stimulation

In order to investigate the effects a stroke can have on contralateral cortical stimulation, solutions were obtained for the stroke model 5 and the healthy head model where the coil was placed at locations of increasing distance from the removed

hemisphere on the contralateral scalp surface, at points Sup3.0, Sup2.0, A3, B3, C3, D3, E3, F3, G3, and H3.

Results

Model convergence (for supplementary material)

Every model converged below the 1.0% energy error stopping criteria. The average number of tetrahedron for the 50 healthy head model solutions was 168,471, and 179,311 for the Stroke 01 solutions, 148,001 for the Stroke 2A–Stroke 4C solutions, and 142,403 for the Stroke 05 solutions. Multiple machines, of varied computing resources, were used in the solution process; however, typical convergence times for a dual 3 GHz Xeon processor machine with 4 Gigs of Ram were as follows: 2:51:44 for the healthy head model with the coil in the C3 position, 2:57:38 for the Stroke 01 model with the coil in the C3 position, and 2:42:39 for the Stroke 05 model with the coil in the C3 position.

Effects of relative coil location on the induced stimulating currents

For the healthy head model, the maximum cortical current densities ranged from 1.45 to 4.35 A/m^2. The maximum cortical current surface areas, defined as the cortical surface area where the current ranged from 90% to 100% of its maximum, ranged in area from a focal 37 mm^2 to wide spotty areas equal to or in excess of 200 mm^2. For all of the solutions, the location of the maximum cortical current density did not correspond directly to the location of the normal projection from figure of eight coil's center, but the projection intersected the cortex within the maximum cortical current surface area. The induced current density variation and vector behavior seen in the tissues were consistent with those of previous studies where the vector orientation followed a figure eight path with the greatest irregularity at the tissue boundaries (Branston and Tofts, 1991; Ueno et al., 1988; Wagner et al., 2004). In Appendix, Table 2-S, of the supplementary material, the magnitude, location, and area of the maximum cortical current densities are tabulated for the 50 coil positions tested in the healthy head model.

When compared to the healthy head model, the current density distributions in the region of the maximum current density were similar in the healthy head model and Stroke 01 model for only the Sup3.0, Sup2.0, Ant3.0, and Ant2.0 coil positions. For these solutions, the locations of the maximum cortical current density were found within 1.5 mm to 2.6 mm of the locations of the maximum cortical current density in the healthy head model and differed in magnitude from −6.1% to 5.1% of the maximum magnitude in the healthy head model.

However, the current density distributions of the Stroke 01 model were considerably altered for the remaining 46 out of the 50 coil positions tested as compared with the healthy head model; whereby, the maximum magnitude, maximum location, and current vector orientations of the induced current density were altered in the stroke model. For these solutions, the maximum cortical current density was systematically found along the stroke borders within ±1 mm of one of the eight discrete locations; the superior anterior stroke border (SASB), superior midline stroke border (SMSB), superior posterior stroke border (SPSB), inferior anterior stroke border (IASB), inferior anterior to midline stroke border (IAMSB), inferior midline stroke border (IMSB), inferior posterior to midline stroke border (IPMSB), and the inferior posterior stroke border (IASB) (see Fig. 2A, which defines all of these locations and others referenced in this paper). These maximum cortical current density locations ranged from 3.8 to 28.5 mm distant from the corresponding location in the healthy head model and were generally located at the corner location along the stroke border that was most proximal to the figure of eight coil's center. Exceptions were found in cases where the maximum was located along the edge of the most proximal stroke border location instead of at a stroke corner location. Additionally, the maximums for the three most posterior coil positions evaluated along the E line (E1, E2, and E3) were located at the SPSB even though the inferior border was more proximal to the coil center (see Appendix, Table 2-S). For these 46 coil positions, the cortical current density magnitudes were consistently larger than those found in the healthy head model, ranging from 1.85 to 7.42 A/m^2, while the differences between the healthy head and Stroke 1 models ranged from 12.8% to 187.8% (these results are tabulated for all of the coil positions in Appendix, Table 2-S).

The maximum current density in the stroke cases for these 46 coil positions was localized to discrete focal sites along the infarction border. The maximum cortical current surface areas for these solutions were more focal than those of the healthy head model, ranging in area from less than 10 mm^2 to 77 mm^2, tabulated in Appendix, Table 2-S (i.e., the maximum cortical surface area was defined as the surface area on the cortex where the current density was greater than 90% of its maximum). Despite this result, the areas in the stroke models, where the current density magnitude was in excess of the corresponding healthy head maximum, were much larger in area than these maximum cortical current density areas. Moreover, the areas in the stroke models where the current density magnitude was in excess of the corresponding healthy head maximum extended well beyond the discrete locations identified as the maximum point locations. For each of these 46 coil positions, there were at least two areas in the Stroke 01 model where the cortical current density was greater than the maximum cortical current density of the corresponding healthy head solution, ranging in surface area from less than 10 mm^2 to as high as 284 mm^2. For example, in Fig. 2B for the B4 coil position, there were 3 locations where the current density magnitude in the Stroke 1 model was greater than the maximum current density in the healthy head model. The first one was located along the upper stroke border from the SASB to the SMSB (both inside and outside the cortical cut) with an area of 57 mm^2 and a maximum current density magnitude of 3.48 A/m. The second one was located at the SPSB with an area of 9 mm^2 and maximum current density magnitude of 2.77 A/m^2. And the third was located at the MASB with a 5-mm^2 area and a 2.36-A/m^2 magnitude. Five additional graphical examples are provided in Figs. 2B and C, including the analysis for areas in the Stroke 01 model where the current density was greater than 120% and 150% of maximum in the corresponding healthy head model. Appendix, Table 2-S tabulates the averaged area information.

The induced current density distributions showed the greatest variation along the tissue boundaries, as had been reported earlier in a similar model (Wagner et al., 2004) and in a saline phantom model (Yunokuchi et al., 1998). In the stroke model, the current density vector distributions deviated from predictable figure of eight distributions that were seen in the healthy head model to conform to the infarction boundaries such that the current vectors became more perpendicular to the stroke boundary along its border and particularly focused at the corners where the areas of

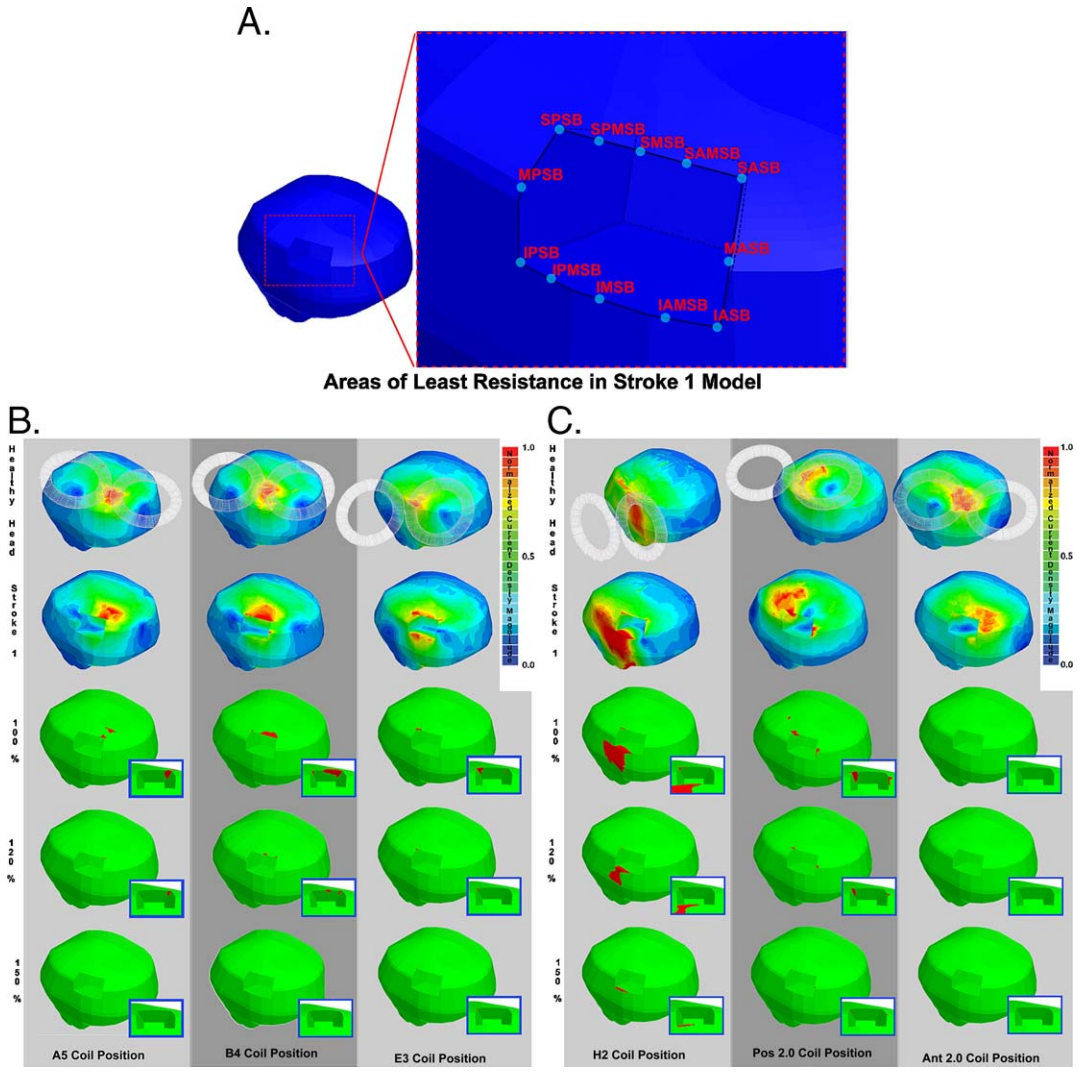

Fig. 2. (A) The areas of least resistance in the Stroke 01 model were found along the edge of the infarction region. The maximum cortical current density and center points of the areas of perturbation were found within ±1 mm of one of these eight locations for 46 of the 50 coil positions tested. They included SASB at (−24.7, 9.0, −16.6), SMSB at (−18.7, −4.2, −16.0), SPSB at (−15.1, −20.5, −17.0), IASB at (−11, 16.4, −35.5), IAMSB at (−9, 11, −35.3), IMSB at (−4, −1.5, −35.3), IPMSB at (−3, −6, −35.4), IASB at (−11, 16.4, −35.5), MASB at (−15.6, 16.5, −22.7), the SPMSB at (−18.2, −9, −16.2), and the SAMSB at (−22.2, 3.1, −16.2). (B) Current density magnitudes and perturbations for the A5, B4, and E3 coil positions. The top plot of each column is that of the current density magnitude for the corresponding healthy head model, note that the scale is normalized to the corresponding healthy head model maximum current density magnitude. The second plot is that of the current density magnitude for the Stroke 01 model, note that the scale is normalized to the maximum of the current density magnitude of the healthy head model such that everything above the maximum in the corresponding healthy head model is shown in bright red to highlight the perturbation effect. The third plot is that of the current density magnitude in the Stroke 01 model which is greater than the maximum current density magnitude of the healthy head model (shown in red). The fourth plot is that of the current density magnitude in the Stroke 01 model which is greater than 120% of the maximum current density magnitude of the healthy head model (shown in red). The fifth plot is that of the current density magnitude in the Stroke 01 model which is greater than 150% of the maximum current density magnitude of the healthy head model (shown in red). (C) Current density magnitudes and perturbations for the H2, Pos 2.0, and Ant 2.0 coil positions. The top plot of each column is that of the current density magnitude for the corresponding healthy head model, note that the scale is normalized to the corresponding healthy head model maximum current density magnitude. The second plot is that of the current density magnitude for the Stroke 01 model, note that the scale is normalized to the maximum of the current density magnitude of the healthy head model such that everything above the maximum in the corresponding healthy head model is shown in bright red to highlight the perturbation effect. The third plot is that of the current density magnitude in the Stroke 01 model which is greater than the maximum current density magnitude of the healthy head model (shown in red). The fourth plot is that of the current density magnitude in the Stroke 01 model which is greater than 120% of the maximum current density magnitude of the healthy head model (shown in red). The fifth plot is that of the current density magnitude in the Stroke 01 model which is greater than 150% of the maximum current density magnitude of the healthy head model (shown in red).

maximum cortical current density were found. For example, in Fig. 3, the vector behavior is graphically displayed for the healthy head and Stroke 01 model for the E3 coil position. The altered directions of current vectors along the stroke borders are evident where vectors deviate in direction perpendicular to the stroke borders. Greater deviations are found along the anterior border and into the corner points along the stroke border, most noticeably as the SPSB and SASB. Additionally, the current vector behavior in the CSF

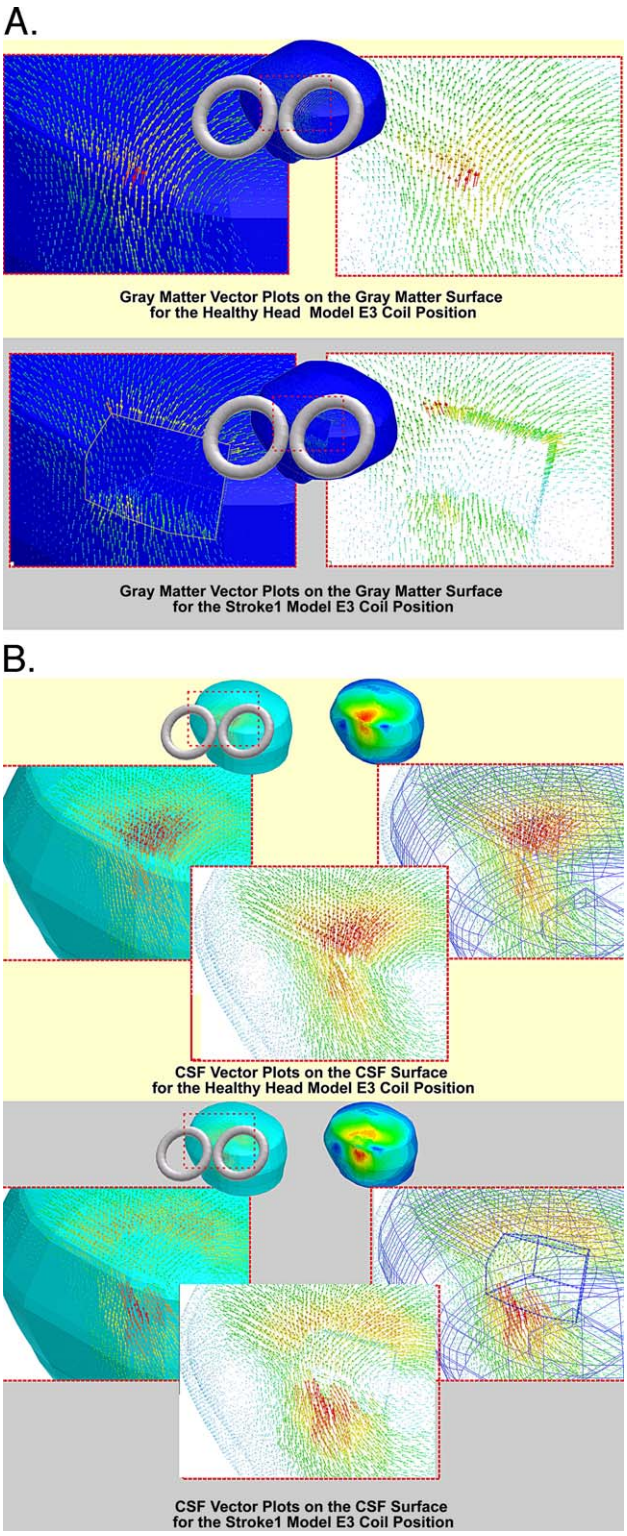

Fig. 3. (A) Current density vector plots on the gray matter surface for the healthy head model and the Stroke 01 model for the E3 coil position. (B) Current density vector plots on the CSF surface for the healthy head model and the Stroke 01 model for the E3 coil position.

showed a similar type of perturbation. Although more subtle in the CSF, the current was still directed from its predictable course in the healthy head models towards the underlying stroke borders. In Fig. 3B, the current density vector distribution in the CSF is plotted for the healthy head model and the Stroke 01 model with the coil in the E3 position.

In the solutions with little to no perturbation (the Sup3.0, Sup2.0, Ant3.0, and Ant2.0 coil positions), the current density was attenuated, and the current vector distribution was oriented tangent to the infarction border at the impending infarction region in the corresponding healthy head model. This could most easily be seen when one compares the Ant2.0 to the Pos2.0 solutions, see Fig. 4. The relative coil to head geometry was such that Ant 2.0 current distribution was localized to a region removed from the stroke border, and the current density distribution in the healthy head model was sufficiently attenuated at the location of the infarction site in the Stroke 01 model. The current density magnitude decayed to 44.0% of its maximum at a point 0.5 cm posterior to the anterior stroke border and 0.5 cm inferior to the location of the superior stroke border in the corresponding healthy head solution. However, for the Pos 2.0 solution, the current density distribution was not sufficiently attenuated at the location of the infarction site in the Stroke 01 model, decaying to 73.6% of its maximum at a point 0.5 cm anterior to the posterior stroke border and 0.5 cm inferior to the superior stroke border in the corresponding healthy head solution. Additionally, when comparing the vector orientations of these two coil positions for both the healthy head model and the Stroke 01 model, the vector current orientation of the healthy head model was approximately normal to the location where the nearest infarction border was found in the Stroke 01 model for the Pos 2.0 solutions, and the vector current orientation of the healthy head model was approximately parallel to the location where the nearest infarction border was found in the Stroke 01 model for the Ant2.0 solutions.

The degree of perturbation, both in area and magnitude, for the Stroke 01 model was clearly dependent on the coil location. The relative head geometry/curvature, relative coil to infarction position, and which infarction border/discrete maximum current density location was closest to the coil center (or the parallel edge of the coil border when the center was distant) were the most obvious factors influencing the degree of perturbation. The eight discrete locations along the infarction border where the current maximums were found appear to correspond to areas of least resistance in the Stroke 01 model. On average, the largest areas of perturbation and percent of differences between the healthy head model and the Stroke 01 model were found along the inferior stroke border; these were found for the coil positions located along the flatter temporal face of the head where less focal distributions were seen in the corresponding healthy head model. As the source position and model (Stroke 01 vs. healthy head model) changed the distributions obviously changed, but the largest degrees of perturbation were generally seen when the distribution in the healthy head model was such that the current density vector distribution was oriented normal to the location where the stroke border was found in the corresponding Stroke 01 model.

Effects of the infarction shape on the induced stimulating currents

Herein, we focus on the differences between the Stroke 2A through the Stroke 4C models based on their geometries. Although similar trends were seen in the analysis of the Stroke 2A–Stroke 4C models as were seen in the Stroke 1 models regarding the degree of perturbation, the current vector behavior, areas of least resistance, and boundary effects, we limit their reporting here to highlight the major differences seen between the Stroke 2A and Stroke 4C models.

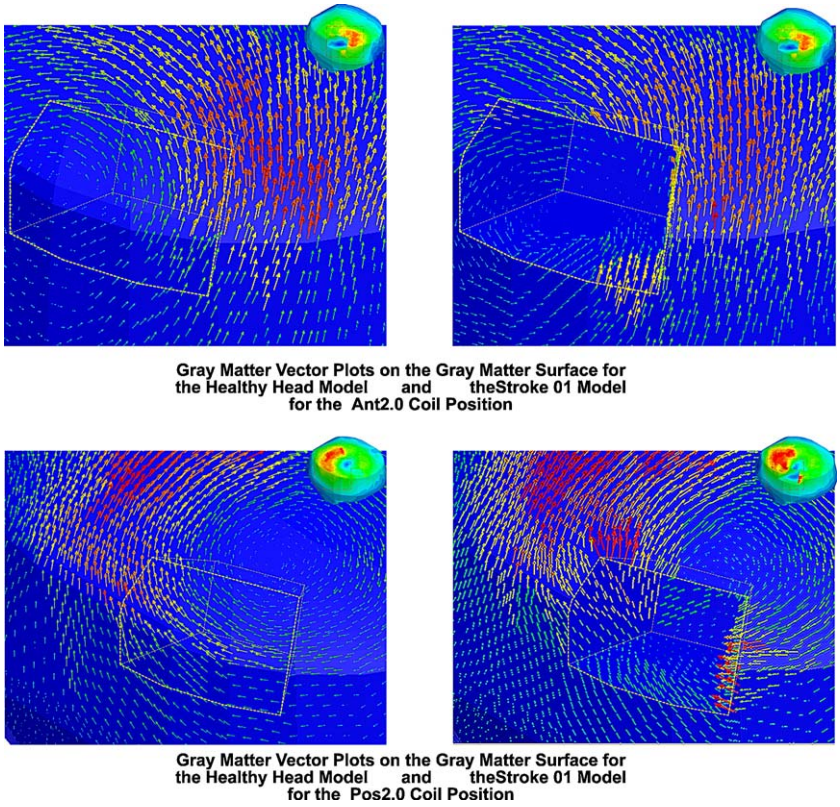

Fig. 4. Current density vector plots on the gray matter surface for the healthy head and the Stroke 01 models for the Ant 2.0 and Pos 2.0 coil positions. Note that the stroke border is projected on the surface of the gray matter in the healthy head model to display its impending location (outlined in yellow). In the Pos 2.0 coil position, the current density vectors are oriented approximately normal to the projected stroke border in the healthy head model where the maximum perturbation is found in the corresponding Stroke 01 model. In the Ant 2.0 coil position, the current density vectors are approximately parallel to the stroke border closest to the coil center, and that the level of perturbation along the stroke border does not exceed the maximum in the corresponding healthy head model.

The difference between the maximum current density magnitudes in the healthy head model and the corresponding stroke model got larger as the stroke depth got larger. Conversely, as the stroke shapes increased in anterior to posterior width, the magnitude differences between the healthy head model and the corresponding stroke got smaller. In general, as the stroke border got larger in width and/or depth, the areas of perturbation got larger. The results are tabulated in Appendix, Table 2-S of the supplementary materials section.

Effects of contralateral hemisphere stimulation

The percent of difference between the maximum current density in the healthy head and the stroke model decreased with increasing coil distance from the infarcted hemisphere. For all of the Stroke 5 coil positions, except for that of the Sup3.0 position, there was only one area of perturbation for each position where the current density magnitude exceeded the maximum current density in the corresponding healthy head model (corresponding to the location of the new maximum); this area of perturbation decreased with increasing distance from the infarcted hemisphere. Additionally, for every coil position, except for the Sup3.0 coil position, the location of the coil density maximum was within ±2 mm of the maximum location in the corresponding healthy head model. For the Sup3.0 position, there were 2 areas of perturbation which exceeded 100% of the maximum in the corresponding healthy head model: at the location of the maximum cortical current density and where the maximum cortical current density was located in the corresponding healthy head model.

Similar vector behavior was seen in both the healthy head and stroke model for all of the solutions along the cortical surface except at the hemisphere border. These variations became more pronounced as the percent of difference between the models increased (i.e., the distances between the coil and the hemispherectomy diminished). The current vectors were oriented in a more perpendicular direction along the hemisphere border than they were oriented in the corresponding locations in the healthy head model. Appendix, Table 2-S in the supplementary materials section tabulates the results from these models. Fig. 5 plots the percent of difference between the healthy head model and the Stroke 5 model vs. increasing coil distance from the stroke boundary.

Discussion

This paper explores the effect that electrical and anatomical changes caused by stroke have on the TMS induced electrical currents in the brain. Our models are based on a finite element electromagnetic solver integrated with MRI derived head models. Comparisons of the healthy head model with previous studies are

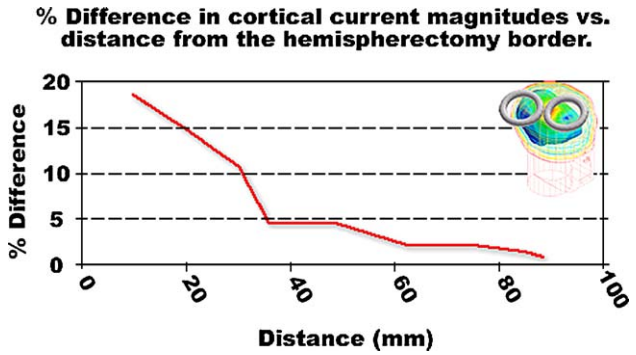

Fig. 5. Percent of difference between the maximum cortical current density in the stroke and healthy head model as a function of coil center distance from the hemispherectomy border.

discussed in detail in an earlier publication (Wagner et al., 2004), and herein, we focus on the difference between the healthy head model and the stroke models. We show that the disruption due to a stroke can drastically modify the effect of TMS in several ways: (1) it alters the location of the maximum cortical current density, (2) it alters the magnitude and distribution of the induced currents, and (3) it modifies the focus of stimulation, all of which will alter the population of neural elements stimulated and ultimately lead to clinical implications, which are discussed below.

Altered location of maximum cortical current density

This study demonstrates that in the presence of a chronic, cortical stroke, the predicted location of the maximum current density induced by TMS in the cortex based on conventional models would be inaccurate when stimulation is aimed to a cortical region proximal to the lesion. For the healthy head models, the perpendicular projection from the coil's face center was always within the area of the maximum cortical current. For the stroke models, this was rarely the case; for all of the stroke models where the source coil (figure of eight coil with two 3.5 cm radius windings) was centered within 1 cm of the infarction border, we found sizeable distances between the location of the maximum current density in the stroke and the corresponding healthy head solutions (distances between the corresponding maximums as great as 24.1 mm were observed). However, this is not to say that the maximum location would be unperturbed when the coil center is greater than 1 cm away from the infarction border. For example, in the Stroke 1 model, there were coil positions where the coil center was 2 and 3 cm away from the stroke border in which the maximum location was still significantly altered. Thus, the exact distance will always depend on the coil size, relative coil to scalp angle, and head and infarction geometry.

Nevertheless, our present findings and the results of an earlier study (Wagner et al., 2004) suggest that the current density distribution will not be appreciably altered in cases where the induced distribution is noticeably attenuated at the corresponding location in the healthy head model (in our studies, the induced current density magnitude was found to be less than 50% of the maximum in the corresponding healthy head model at the location of the impending infarction site for cases that did not show a noticeable perturbation). This result was confirmed in all the solutions where the projection of the coil (both its center and border regions) onto the cortex did not overlap with the underlying infarction border (see the Stroke 5 results).

Altered magnitude of maximum cortical current density

The analysis also indicates that the magnitude of the induced current density is altered following a stroke, and that the magnitude calculated in healthy cortex is an inadequate predictor of the levels expected in pathological cases. Our modeling results suggest that the influx of CSF into the infarction region following a stroke essentially creates a new shunting route for the currents to follow. The CSF is far more conductive than the surrounding brain tissue, and thus, areas of least resistance appear to attract the current along the border of the infarction. Depending on the stroke geometry and coil location, multiple areas of least resistance may appear. These tend to be at corner points of the stroke boundary, a result often seen in the analysis of eddy currents at 90° corner points (Deeley, 1990).

The current density difference between the healthy head model and the stroke models is large in especially focal regions (as high as 188% in the Stroke 01 model for the G5 coil position). However, for some of these very focal areas of maximum cortical current density, the extreme perturbations would most likely have clinically insignificant effects. The rationale underlying this lack of effect is that these areas were confined to either corners or edges along the stroke border and generally spanned areas of less than 10 mm^2 where scar tissue and nonfunctional neural tissue would be found (Dirnagl et al., 1999). Nevertheless, as illustrated by multiple stroke models, these areas can also extend past the infarction border, at locations of presumed viable healthy cortex, such that these perturbations would have clinically significant effects. Additionally, for those models where the areas of maximum cortical current density were small, there were still large regions where the current density distributions were greater than those seen in the corresponding healthy head model—just not as great as the extremes found in the corner points (for instance, in Fig. 2B for the Pos 2.0 coil position, there are three locations where the current density magnitude was greater than the maximum found in the healthy head model ranging in area from 23 to 64 mm^2, yet the area of the maximum cortical current density was just 5 mm^2). Finally, there were numerous stroke solutions where the cortical current density was greater than that seen in the corresponding healthy head model in corresponding regions, even though it did not exceed the absolute maximum.

These changes in the current density magnitude make the use of the MEP threshold unreliable as a TMS safety standard in the affected cortex and ultimately make the case for the pursuit of improved TMS safety standards in the altered cortical tissue. MEP thresholds developed in the region of altered cortical cortex should not be transposed as a reference to other cortical sites (and vice versa).

Altered focus of stimulation

In addition to the potential location and magnitude inaccuracies, the analysis provides evidence that the focus of induced current from TMS will be appreciably diminished following a stroke. In the healthy head model, the maximum cortical current density was always confined to a single discrete cortical location. However, in the stroke models, there were many solutions with multiple disjoint areas, around the infarction border, where the current density was

near its maximum or greater than the maximum seen in the corresponding healthy head models. For example, in Fig. 2B for the B4 coil position, there are two areas separated by approximately 1 cm located at the SASB and the SMSB of 3.48 and 3.23 A/m^2 magnitudes.

Altered network activation

Experimental and modeling data suggest that the site of activation is predicted by the peak electric field and thus, the cortical current density, in the cortical neurons (Nagarajan and Durand, 1995; Nagarajan et al., 1993; Amassian et al., 1992) (Maccabee et al., 1993). For instance Nagarajan and Durand (1995) found for "short axons with sealed ends, excitation is governed by the boundary field driving function which is proportional to the electric field" (Nagarajan et al., 1993). Additionally, Maccabee et al. (1993) state "excitation at the terminations take place at much lower thresholds and it occurs at a site within the peak electric field," (Maccabee et al., 1993) as does excitation at fiber bends of corticospinal and other neurons (note that this is different from the activation site of long (relative to the coil dimensions) straight neurons in the peripheral nervous system, which is predicted well by the first spatial derivative of the induced electric field (Nagarajan and Durand, 1994; Roth and Basser, 1990)). Our data thus suggest that the site of activation will be altered in stroke patients (and in all patients who suffer from pathologies that alter the electrical and anatomical tissue properties proximal to the simulation site).

In addition to the stimulation changes expected due to the new maximum cortical current density magnitude and location, different neural elements would also be activated in stroke patients due to the alteration of the current vector orientations. A modification of the current density vector orientation along the infarction border is predicted from the boundary condition that the normal current density components must be continuous across boundaries. Thus, when one goes from the highly conductive CSF to the less conductive cerebral tissue, the jump in normal components is expected in the stroke models when compared to the healthy head models. This will alter the current density direction along the stroke border, and although there are different theories concerning the direction of the current vectors and which cortical neurons are stimulated (Nagarajan and Durand, 1995; Maccabee et al., 1993; Amassian et al., 1992; Roth and Basser, 1990; Ueno et al., 1990), it is clear that the directionality of the induced currents plays a clear role in which neurons are stimulated (Chiappa, 1994). Thus, different neural elements could be activated in stroke patients than would be predicted in a healthy head.

Clinical implications

The altered location of the maximum cortical current density location is important when TMS is used in the investigation and treatment of patients with stroke (Alagona et al., 2001; Mansur et al., 2005; Pennisi et al., 2002). When TMS is applied over the undamaged hemisphere or the damaged hemisphere (but where the coil is not proximal to the lesion location), the maximum cortical current density location can still be roughly predicted based on the expected results in a healthy head model. However, when targeting regions of the cortex proximal to the lesion site, one would need to account for the perturbation of the maximum current density location. One solution to this problem would be the use of a stereotaxic system integrated with a field solver to predict the location of the maximum cortical current density during stimulation. Otherwise, the inaccuracies in the predicted location of the maximum cortical current density could prove to be dangerous or at the very least provide unpredictable results in behavioral or clinical applications of TMS.

TMS safety standards based on expected current density distributions for healthy cortices should not be applied in the altered cortical tissue. For example, it has been noted that stroke and other pathologies could lower the TMS seizure threshold in patients (Anand and Hotson, 2002), and, in cases where the pathological tissue leads to amplification of the induced current density magnitudes, the dangers are obviously magnified and the likelihood of seizure is increased. Additionally, as discussed above, the changes in the current density magnitude make the use of the MEP threshold unreliable as a TMS safety standard in the effected cortex, as has been recommended in studies where current perturbations are not expected (Wassermann, 1998).

Overall, the demonstrated cortical current perturbations should be considered when interpreting clinical TMS studies of stroke. For example, in the area of brain plasticity, TMS has been one of the tools used to demonstrate changes in motor map size, location, and excitability after brain lesions such as stroke. For instance, Delvaux et al. (2003), studying 31 patients who experienced an ischemic stroke in the middle cerebral artery territory, showed that persistence of MEP on the affected side just after the onset of the stroke was a strong predictor of good recovery (Delvaux et al., 2003). Furthermore, the authors observed a significant displacement of center of gravity of motor maps towards more frontal regions on the affected side, while no change was noted on the unaffected side. Our results suggest that TMS-based studies of cortical changes following a stroke can be influenced by the disturbance of the induced electric current caused by physiological changes to the lesion area. Therefore, these patients may not have presented MEPs not because of the lesion characteristics but because the induced stimulating current disturbance caused by the lesion. This is not to say that MEP measurements cannot provide a gauge of the remaining viable corticospinal projections, but ultimately, a clinical prognosis based on the MEP response should take into account the effect of the lesion on the induced electric current by TMS.

Another area where the current perturbations need to be considered is in the field of TMS induced neuro-rehabilitation. TMS stimulation has been proposed as a tool to affect plasticity in stroke patients (Mottaghy, 2003). The neuro-rehabilitative capacities of TMS have been demonstrated in the undamaged hemisphere in stroke patients (Mansur et al., 2005; Martin et al., 2004; Oliveri et al., 1999). However, there have not been any studies that offer clear results with stimulation focused in the lesion region. This is quite possibly due to limitations of the current density perturbations. In future studies focused on stimulation of the infracted cortex, the perturbations will need to be accounted for, preferably in a stroke by stroke basis, due to the unique geometry of each infarction. The fact that the degree and location of perturbation will be uniquely determined by the relative lesion shape to coil position means that the perturbations should be accounted for with a stereotactic system integrated with an MRI-based field solver which accounts for the tissue changes. Systems which predict the location of stimulation based on the perpendicular projection from the coil face will not be accurate.

Additionally, systems that transpose perfect sphere models or homogenous geometries onto MRI-based trackers will suffer from the same unreliability.

If the stereotactic field solver technology is not available, there are no simple rules of thumb which will predict the exact perturbations expected. However, from this model, one could expect the currents to be amplified on the stroke border proximal to the coil boundary, especially at locations where there are sharp demarcations in the tissue type. For instance, in our model, sharp edges on the stroke border seemed to serve as areas of least resistance. Oftentimes, we found that the areas of elevated current magnitude extended from the expected stimulation location to these areas of least resistance on the lesion border with the largest perturbations proximal to the figure of eight coil's center. However, cases were found where the outer edge of the coil was proximal to the largest perturbations, especially when the coil was positioned such that the currents were oriented normal to the stroke interface. As such, one would prefer to place the coil such that no part of it was overlying the stroke border in order to minimize the perturbations.

In addition to these generalizations, there are a number of precautions that should be taken. While the MEP measurements can still provide a measure of cortical viability following a stroke, comparisons between the two hemispheres should be avoided (i.e., data from the nonaffected hemisphere tell one nothing as to the current distributions in the peri-lesional region). Predictions of the precise targeting of focal cortical regions based on the surface coil position should not be made if the coil is placed proximal to the infarction site. Finally, comparisons between cortical and sub-cortical strokes should be viewed skeptically if the region of stimulation is proximal to the cortical or sub-cortical lesion (even though sub-cortical strokes have not been presented in this study, the authors believe that alterations of the current density distributions will occur if the infarctions are not too distal from the cortical surface).

The stimulating induced current density distributions are clearly altered following a cerebrovascular event that damages the cortex in such a way that the tissue geometry and conductive properties are modified. Even though we focused on the perturbations caused by strokes in this paper, similar changes will be seen for any pathology that alters the cortical anatomy or the electric tissue properties. For example, CSF fills the void caused by the cerebral atrophy, much like is seen in stroke, and thus, TMS induced stimulating currents could be altered in atrophic cortices as predicted by these stroke models (dependent upon the degree and location of atrophy). It is also possible that large sulci could cause similar current perturbations in healthy individuals; however, further study needs to be conducted in this area. The influx of CSF is not the only type of disturbance that will cause such current perturbations. For example, the conductivity of tissue is altered (Smith et al., 1986) in the presence of a tumor, and, thus, one could see current density perturbations if the tumor was found in the region of stimulation. In actuality, in the presence of any pathology, one cannot accurately predict the site, magnitude, and effects of TMS-based on healthy head models.

Study limitations

Some limitations of this study suggest specific areas of possible future research. First, the resolution of the model is limited by the CAD rendering of the human head and does not share the same resolution as the MRI that was used to derive it. Additionally, further research needs to be completed on the low-frequency tissue electrical properties to account for their dispersive properties, anisotropies, and heterogeneities. The model should be expanded in the future to account for these tissue properties as more data become available. Another limitation requiring further exploration comes from the fact that true stroke lesions have irregular borders and shapes that were not completely reproduced by our model. Although this could alter the effects of TMS on the lesion site, we believe that this effect did not interfere with the results of our simulation. The main effect observed in this study can be attributed to the shunting caused by the CSF, and this quantity was not affected by our model reconstruction. Another possible limitation of this modeling framework concerns the solution technique FEM solvers employ near corner regions (Park et al., 1995; Preis et al., 2000). For a T-omega solver, the worst case solution in the study of Preis et al. (2000), comparing different solution techniques, showed a current density magnitude that was underreported at the reentrant corner point by approximately 25% (Preis et al., 2000). In order to minimize this potential effect, the FEM mesh density was increased along the stroke border, and the analysis was expanded to include regions far from the corner points. Additionally, as indicated in the text above, stimulation in the corner regions along the stroke border most likely has no clinical effect due to the scarring and presence of necrotic tissue, implying that these corner effects will have a negligible effect clinically. Finally, some of the general trends that we saw in the analysis of the effects of the infarction size on the induced stimulating currents are difficult to extrapolate to broad real world trends; although we saw an increase of perturbation with an increase in infarction depth, and the inverse effect with the increased width of the anterior to posterior stroke size, a more complete analysis would need to be pursued with a randomized model of stroke shapes and coil positions to see if these general trends are truly shape dependent. Most likely, with the complexity of the system, every stroke shape will uniquely influence the current perturbations such that the general trends in the perturbation will be difficult to produce in a standardized way.

Conclusions

This study demonstrates that TMS effects cannot be predicted in stroke patients by conventional methods based on healthy head models, when TMS is applied to damaged areas. The kind of perturbations observed in the stroke models will occur in other pathological cases in which the geometry or electrical characteristics of brain tissue are altered. These cortical current density perturbations could prove to be dangerous or at the very least lead to unreliable, erroneous results if guided by models that do not account for the electromagnetic tissue interactions. Future efforts and model refinements will help to further increase our understanding of the mechanisms of TMS in stroke.

Acknowledgments

We acknowledge the contribution of the Maxwell software from the Ansoft Corporation, Pittsburgh, PA, that was used in

this study. This work was supported part by the Center for Integration of Medicine and Innovative Technology under Grant Numbers 45335 and 20736 and NIH Grants RO1 EB005047, RO1 DC05672, RO1 NS20068, K24 RR018875. In addition, F.F. received support under a grant from the Harvard Medical School Scholars in Clinical Sciences Program (NIH K30 HL04095-03).

Appendix A. Supplementary data

Supplementary data associated with this article can be found in the online version at doi:10.1016/j.neuroimage.2005.04.046.

References

Akhtari, M., Bryant, H.C., Mamelak, A.N., et al., 2002. Conductivities of three-layer live human skull. Brain Topogr. 14, 151–167.

Alagona, G., Delvaux, V., Gerard, P., et al., 2001. Ipsilateral motor responses to focal transcranial magnetic stimulation in healthy subjects and acute-stroke patients. Stroke 32, 1304–1309.

Amassian, V., Eberle, L., Maccabee, P., Cracco, R., 1992. Modeling magnetic coil excitation of human cerebral cortex with a peripheral nerve immersed in a brain-shape volume conductor: the significance of fiber bending in excitation. Electroencephalogr. Clin. Neurophysiol. 85, 291–301.

Anand, S., Hotson, J., 2002. Transcranial magnetic stimulation: neurophysiological applications and safety. Brain Cogn. 50, 366–386.

Ansoft, 1990a. Eddy Axial Current. Ansoft, Pittsburgh.

Ansoft, 1990b. Eddy Axisymmetric. Ansoft Corporation, Pittsburgh.

Ansoft, 2002. Maxwell 3 D, 9th ed. Ansoft, Pittsburgh.

Arac, N., Sagduyu, A., Binai, S., Ertekin, C., 1994. Prognostic value of transcranial magnetic stimulation in acute stroke. Stroke 25, 2183–2186.

Berardelli, A., 1991. Electrical and magnetic spinal and cortical stimulation in man. Curr. Opin. Neurol. Neurosurg. 4, 770–776.

Bohning, D.E., Pecheny, A.P., Epstein, C.M., et al., 1997. Mapping transcranial magnetic stimulation (TMS) fields in vivo with MRI. NeuroReport 8, 2535–2538.

Branston, N.M., Tofts, P.S., 1991. Analysis of the distribution of currents induced by magnetic field in a volume conductor. Phys. Med. Biol. 36, 161–168.

Burger, H.C., Van Milaan, J.B., 1943. Measurement of the specific resistance of the human body to direct current. Acta Med. Scand. 114, 584–607.

Byrnes, M.L., Thickbroom, G.W., Phillips, B.A., Wilson, S.A., Mastaglia, F.L., 1999. Physiological studies of the corticomotor projection to the hand after subcortical stroke. Clin. Neurophysiol. 110, 487–498.

Cerri, G., De Leo, R., Moglie, F., Schiavoni, A., 1995. An accurate 3-D model for magnetic stimulation of the brain cortex. J. Med. Eng. Tech. 19, 7–16.

Chiappa, K.H., 1994. Transcranial motor evoked potentials. Electromyogr. Clin. Neurophysiol. 34, 15–21.

Cicinelli, P., Traversa, R., Bassi, A., Scivoletto, G., Rossini, P.M., 1997. Interhemispheric differences of hand muscle representation in human motor cortex. Muscle Nerve 20, 535–542.

Crille, G.W., Hosmer, H.R., Rowland, A.F., 1922. The electrical conductivity of animal tissues under normal and pathological conditions. Am. J. Physiol. 60, 59–106.

Cruz Martinez, A., Tejada, J., Diez Tejedor, E., 1999. Motor hand recovery after stroke. Prognostic yield of early transcranial magnetic stimulation. Electromyogr. Clin. Neurophysiol. 39, 405–410.

D'Olhaberriague, L., Espadaler Gamissans, J.M., Marrugat, J., Valls, A., Oliveras Ley, C., Seoane, J.L., 1997. Transcranial magnetic stimulation as a prognostic tool in stroke. J. Neurol. Sci. 147, 73–80.

Dachy, B., Dan, B., 2002. Electrophysiological assessment of the effect of intrathecal baclofen in spastic children. Clin. Neurophysiol. 113, 336–340.

Dachy, B., Biltiau, E., Bouillot, E., Dan, B., Deltenre, P., 2003. Facilitation of motor evoked potentials in ischemic stroke patients: prognostic value and neurophysiologic correlations. Clin. Neurophysiol. 114, 2370–2375.

De Girolami, U., Anthony, D.C., Frosch, M.P., 1999. Cerebrovacular diseases. In: Cotran, R.S., Kumar, V., Collins, T. (Eds.), Robbins Pathological Basis of Disease. W.B. Saunders Company, Philadelphia, pp. 1306–1314.

De Mercato, G., Garcia Sanchez, F.J., 1992. Correlation between low-frequency electric conductivity and permittivity in the diaphysis of bovine femoral bone. IEEE Trans. Biomed. Eng. 39 (5), 523–526.

Deeley, E.M., 1990. Surface impedance near edges and corners in three-dimensional media. IEEE Trans. Magn. 26, 712–714.

Delvaux, V., Alagona, G., Gerard, P., De Pasqua, V., Pennisi, G., de Noordhout, A.M., 2003. Post-stroke reorganization of hand motor area: a 1-year prospective follow-up with focal transcranial magnetic stimulation. Clin. Neurophysiol. 114, 1217–1225.

Dirnagl, U., Iadecola, C., Moskowitz, M.A., 1999. Pathobiology of ischaemic stroke: an integrated view. Trends Neurosci. 22, 391–397.

Dissado, L.A., 1990. A fractal interpertation of the dielectric response of animal tissues. Phys. Med. Biol. 35, 1487–1503.

Eisen, A.A., Shtybel, W., 1990. AAEM minimonograph #35: clinical experience with transcranial magnetic stimulation. Muscle Nerve 13, 995–1011.

Escudero, J.V., Sancho, J., Bautista, D., Escudero, M., Lopez-Trigo, J., 1998. Prognostic value of motor evoked potential obtained by transcranial magnetic brain stimulation in motor function recovery in patients with acute ischemic stroke. Stroke 29, 1854–1859.

Ferbert, A., Buchner, H., 1991. Evoked potentials in diagnosis of ischemic brain stem lesions. Nervenarzt 62, 460–466.

Foster, K.R., Schwan, H.P., 1996. Dielectric properties of tissues. In: Polk, C., Postow, E. (Eds.), Biological Effects of Electromagnetic Fields. CRC Press, New York, pp. 25–102.

Freygang, W.H., Landau, W.M., 1955. Some relations between resistivity and electrical activity in the cerebral cortex of the cat. J. Cell Comp. Physiol. 45, 377–392.

Gabriel, C., Gabriel, S. (1996). Compilation of the dielectric properties of body tissues at RF and microwave frequencies. San Antonio: Air Force Material Command, Brooks Air Force Base, TX.

Gangitano, M., Valero-Cabre, A., Tormos, J.M., Mottaghy, F.M., Romero, J.R., Pascual-Leone, A., 2002. Modulation of input-output curves by low and high frequency repetitive transcranial magnetic stimulation of the motor cortex. Clin. Neurophysiol. 113, 1249–1257.

Geddes, L.A., 1987. Optimal stimulus duration for extracranial cortical stimulation. Neurosurgery 20, 94–99.

Gomez-Fernandez, L., 2000. Cortical plasticity and restoration of neurologic functions: an update on this topic. Rev. Neurol. 31, 749–756.

Hart, F.X., Toll, R.B., Berner, N.J., Bennett, N.H., 1996. The low frequency dielectric properties of octopus arm muscle measured in vivo. Phys. Med. Biol. 41, 2043–2052.

Hasted, J.B., 1973. Aqueous Dielectrics, 1th ed. Halsted Press, New York.

Hendricks, H.T., Zwarts, M.J., Plat, E.F., van Limbeek, J., 2002. Systematic review for the early prediction of motor and functional outcome after stroke by using motor-evoked potentials. Arch. Phys. Med. Rehabil. 83, 1303–1308.

Hilgetag, C.C., Theoret, H., Pascual-Leone, A., 2001. Enhanced visual spatial attention ipsilateral to rTMS-induced 'virtual lesions' of human parietal cortex. Nat. Neurosci. 4, 953–957.

Jacobs, M.A., Zhang, Z.G., Knight, R.A., et al., 2001. A model for multiparametric mri tissue characterization in experimental cerebral ischemia with histological validation in rat: part 1. Stroke 32, 943–949.

Jalinous, R., 1991. Technical and practical aspects of magnetic nerve stimulation. J. Clin. Neurophysiol. 8, 10–25.

Kosslyn, S.M., Pascual-Leone, A., Felician, O., et al., 1999. The role of area 17 in visual imagery: convergent evidence from PET and rTMS. Science 284, 167–170.

Lepeschkin, E., 1951. Modern Electrophysiology, vol. 1. Williams and Wilkins, Baltimore.

Liu, R., Ueno, S., 2000. Calculating the activating function of nerve excitation in inhomogeneous volume conductor during magnetic stimulation using the finite element method. IEEE Trans. Magn. 36, 1796–1799.

Maccabee, P., Amassian, V., Eberle, L., Cracco, R., 1993. Magnetic coil stimulation of straight and bent amphibian and mammallian peripheral nerve in vitro: locus of excitation. J. Physiol. 460, 201–219.

Magstim. New York, New York.

Mansur, C.G., Fregni, F., Boggio, P.S., Riberto, M., Gallucci-Neto, J., Santos, C.M., Wagner, T., Rigonatti, S.P., Marcolin, M.A., Pascual-Leone, A., 2005. A sham-stimulation controlled trial of rTMS of the unaffected hemisphere in stroke patients. Neurology 64 (10), 1802–1804.

Martin, P.I., Naeser, M.A., Theoret, H., et al., 2004. Transcranial magnetic stimulation as a complementary treatment for aphasia. Semin. Speech Lang. 25, 181–191.

Mottaghy, F.M., 2003. TMS: using brain plasticity to treat chronic poststroke symptoms. Neurology 61, 881–882.

Muellbacher, W., Mamoli, B., 1995. Prognostic value of transcranial magnetic stimulation in acute stroke. Stroke 26, 1962–1963.

Nagarajan, S., Durand, D.M., 1994. A general theory for predicting subthreshold transmembrane response to electric and magnetic fields. Engineering Advances: New Opportunities for Biomedical Engineers, vol. 2. IEEE, pp. 770–771.

Nagarajan, S., Durand, D.M., 1995. Analysis of magnetic stimulation of a concentric axon in a nerve bundle. IEEE Trans. Biomed. Eng. 42, 926–933.

Nagarajan, S., Durand, D.M., Warman, E.N., 1993. Effects of induced electric fields on finite neuronal structures: a simulation study. IEEE Trans. Biomed. Eng. 40, 1175–1188.

Nardone, R., Tezzon, F., 2002. Inhibitory and excitatory circuits of cerebral cortex after ischaemic stroke: prognostic value of the transcranial magnetic stimulation. Electromyogr. Clin. Neurophysiol. 42, 131–136.

Oliveri, M., Rossini, P.M., Traversa, R., et al., 1999. Left frontal transcranial magnetic stimulation reduces contralesional extinction in patients with unilateral right brain damage. Brain 122 (Pt. 9), 1731–1739.

Oswald, K., 1937. Messung der leitfahigkeit und Dielektrizitatkonstante biologischer Gewebe un Flussigkeiten bei kurzen Wellen. Hochfrequenztech. Elektroakust. 49, 40–49.

Park, Y.G., Chung, T.K., Jung, H.K., Hahn, S.Y., 1995. Three dimensional eddy current computation using the surface impedance method considering geometric singularity. IEEE Trans. Magnet. 31, 1400–1403.

Pascual-Leone, A., Bartres-Faz, D., Keenan, J.P., 1999. Transcranial magnetic stimulation: studying the brain-behaviour relationship by induction of 'virtual lesions'. Philos. Trans. R. Soc. Lond., Ser. B Biol. Sci. 354, 1229–1238.

Pennisi, G., Rapisarda, G., Bella, R., Calabrese, V., Maertens De Noordhout, A., Delwaide, P.J., 1999. Absence of response to early transcranial magnetic stimulation in ischemic stroke patients: prognostic value for hand motor recovery. Stroke 30, 2666–2670.

Pennisi, G., Alagona, G., Rapisarda, G., et al., 2002. Transcranial magnetic stimulation after pure motor stroke. Clin. Neurophysiol. 113, 1536–1543.

Pereon, Y., Aubertin, P., Guiheneuc, P., 1995. Prognostic significance of electrophysiological investigations in stroke patients: somatosensory and motor evoked potentials and sympathetic skin response. Neurophysiol. Clin. 25, 146–157.

Pethig, R., Kell, D.B., 1987. The passive electrical propeties of biological systems: their significance in physiology, biophysics, and biotechnology. Phys. Med. Biol. 32, 933–970.

Preis, K., Biro, O., Ticar, I., 2000. Gauged current vector potential and reentrant corners in the FEM analysis of 3 D eddy currents. IEEE Trans. Magnet. 36, 840–843.

Radvan-Ziemnowicz, J.C., McWilliams, J.C., Kucharski, W.E., 1964. Conductivity versus frequency in human and feline cerebrospinal fluid. In: Werner, Ma. (Ed.), Proc. 17 Ann. Conf. in Med. and Biol. Washington 12, DC.

Ranck, J.B., 1963. Specific impedance of rabbit cerebral cortex. Exp. Neurol. 7, 144–152.

Rapisarda, G., Bastings, E., de Noordhout, A.M., Pennisi, G., Delwaide, P.J., 1996. Can motor recovery in stroke patients be predicted by early transcranial magnetic stimulation? Stroke 27, 2191–2196.

Romero, J.R., Anschel, D., Sparing, R., Gangitano, M., Pascual-Leone, A., 2002. Subthreshold low frequency repetitive transcranial magnetic stimulation selectively decreases facilitation in the motor cortex. Clin. Neurophysiol. 113, 101–107.

Rossini, P.M., 2000. Is transcranial magnetic stimulation of the motor cortex a prognostic tool for motor recovery after stroke? Stroke 31, 1463–1464.

Roth, B., Basser, P., 1990. A model of stimulation of a nerve fiber by electromagnetic induction. IEEE Trans. Biomed. Eng. 37, 588–597.

Schwarz, S., Hacke, W., Schwab, S., 2000. Magnetic evoked potentials in neurocritical care patients with acute brainstem lesions. J. Neurol. Sci. 172, 30–37.

Sironi, L., Guerrini, U., Tremoli, E., et al., 2004. Analysis of pathological events at the onset of brain damage in stroke-prone rats: a proteomics and magnetic resonance imaging approach. J. Neurosci. Res. 78, 115–122.

Smith, S.R., Foster, K.R., Wolf, J.L., 1986. Dielectric properties of vx-2 carcinoma vs. normal liver tissues. IEEE Trans. Biomed. Eng. 33, 522.

Soltanian-Zadeh, H., Pasnoor, M., Hammoud, R., et al., 2003. MRI tissue characterization of experimental cerebral ischemia in rat. J. Magn. Reson. Imag. 17, 398–409.

Starzynski, J., Sawicki, B., Wincenciak, S., Krawczyk, A., Zyss, T., 2002. Simulation of magnetic stimulation of the brain. IEEE Trans. Magn. 38, 1237–1240.

Stulin, I.D., Savchenko, A.Y., Smyalovskii, V.E., et al., 2003. Use of transcranial magnetic stimulation with measurement of motor evoked potentials in the acute period of hemispheric ischemic stroke. Neurosci. Behav. Physiol. 33, 425–429.

Theoret, H., Haque, J., Pascual-Leone, A., 2001. Increased variability of paced finger tapping accuracy following repetitive magnetic stimulation of the cerebellum in humans. Neurosci. Lett. 306, 29–32.

Traversa, R., Cicinelli, P., Pasqualetti, P., Filippi, M., Rossini, P.M., 1998. Follow-up of interhemispheric differences of motor evoked potentials from the 'affected' and 'unaffected' hemispheres in human stroke. Brain Res. 803, 1–8.

Ueno, S., Tashiro, T., Harada, K., 1988. Localised stimulation of neural tissues in the brain by means of a paired configuration of time-varying magnetic fields. J. Appl. Phys. 64, 5862–5864.

Ueno, S., Matsuda, T., Fujiki, M., 1990. Functional mapping of the human motor cortex obtained by focal and vectorial magnetic stimulation of the brain. IEEE Trans. Magn. 26, 1539–1544.

Urban, P.P., Morgenstern, M., Brause, K., et al., 2002. Distribution and course of cortico-respiratory projections for voluntary activation in man. A transcranial magnetic stimulation study in healthy subjects and patients with cerebral ischemia. J. Neurol. 249, 735–744.

Vang, C., Dunbabin, D., Kilpatrick, D., 1999. Correlation between functional and electrophysiological recovery in acute ischemic stroke. Stroke 30, 2126–2130.

Wagner, T.A., Zahn, M., Grodzinsky, A.J., Pascual-Leone, A., 2004. Three-dimensional head model simulation of transcranial magnetic stimulation. IEEE Trans. Biomed. Eng. 51, 1586–1598.

Wassermann, E.M., 1998. Risk and safety of repetitive transcranial magnetic stimulation: report and suggested guidelines from the International Workshop on the Safety of Repetitive Transcranial

Magnetic Stimulation, June 5–7, 1996. Electroencephalogr. Clin. Neurophysiol. 108, 1–16.

Werhahn, K.J., Classen, J., Benecke, R., 1995. The silent period induced by transcranial magnetic stimulation in muscles supplied by cranial nerves: normal data and changes in patients. J. Neurol., Neurosurg. Psychiatry 59, 586–596.

Wittenberg, G.F., Chen, R., Ishii, K., et al., 2003. Constraint-induced therapy in stroke: magnetic-stimulation motor maps and cerebral activation. Neurorehabil. Neural Repair 17, 48–57.

Yunokuchi, K., Kato, R., Yoshida, H., Tamari, Y., Saito, M., 1998. Study on the distributions of induced electric field in an inhomogeneous medium exposed a pulsed magnetic field. Annual International Conference of the IEEE of the Engineering in Medicine and Biology Society, vol. 6, pp. 3294–3297.